C Journal of Carbon Research

MDPI

*Article*

# Thermochemistry of a Biomimetic and Rubisco-Inspired $CO_2$ Capture System from Air

**Andrew Muelleman, Joseph Schell, Spencer Glazer and Rainer Glaser ***

Department of Chemistry, University of Missouri, Columbia, MO 65211, USA;
awmnbb@mail.missouri.edu (A.M.); jrsg24@mail.missouri.edu (J.S.); sbgxc5@mail.missouri.edu (S.G.)
* Correspondence: glaserr@missouri.edu; Tel.: +1-573-882-0331

Academic Editor: Enrico Andreoli
Received: 1 May 2016; Accepted: 21 June 2016; Published: 1 July 2016

**Abstract:** In theoretical studies of chemical reactions the reaction thermochemistry is usually reported for the stoichiometric reaction at standard conditions ($\Delta G^\circ$, $\Delta H^\circ$, $\Delta S^\circ$). We describe the computation of the equilibrium concentrations of the $CO_2$-adducts for the general capture reaction $CO_2$ + Capture System $\rightleftarrows$ $CO_2$-adduct (GCR) and the rubisco-type capture reaction $CO_2$ + Capture System $\rightleftarrows$ $CO_2$-adduct + $H_2O$ (RCR) with consideration of the reaction $CO_2(g) \rightleftarrows CO_2(aq)$ via Henry's law. The resulting equations are evaluated and graphically illustrated as a function of atmospheric $CO_2$ concentration and as a function of temperature. The equations were applied to the thermochemistry of small molecule rubisco-model reactions and series of additional model reactions to illustrate the range of the Gibbs free enthalpy for the effective reversible capture and of the reaction entropy for economic $CO_2$ release at elevated temperature. A favorable capture of free enthalpy is of course a design necessity, but not all exergonic reactions are suitable $CO_2$ capture systems. Successful $CO_2$ capture systems must allow for effective release as well, and this feature is controlled by the reaction entropy. The principle of using a two-pronged capture system to ensure a large negative capture entropy is explained and highlighted in the graphical abstract. It is hoped that the presentation of the numerical examples provides useful guidelines for the design of more efficient capture systems.

**Keywords:** carbon capture; $CO_2$ capture from air; temperature dependence of $CO_2$ release; rubisco model; ab initio theory; thermochemistry; capture reaction Gibbs free enthalpy; capture reaction entropy

## 1. Introduction

Continuous atmospheric $CO_2$ tracking started more than 50 years ago with $CO_2$ measurement at Mauna Loa and resulted in the "Keeling Curve," the iconic demonstration of the seasonal variations of $CO_2$ concentrations and the steady rise of the annual average $CO_2$ concentration [1,2]. NOAA's (National Oceanic and Atmospheric Administration) CarbonTracker [3] employs a global network of $CO_2$ mole fraction observations to study the $CO_2$ exchange between the biosphere and the atmosphere as a function of time [4,5]. Comprehensive carbon inventories have been under development by the US Carbon Cycle Science Program [6] and include space-based $CO_2$ observation (i.e., Orbiting Carbon Observatory, OCO-2 [7]). While considerable uncertainties remain with regard to accounting for all $CO_2$, all reports consistently show that the global atmospheric $CO_2$ concentrations have been growing steadily, and at Mauna Loa the average annual mean increased from 316.0 ppm in 1959 to its value of 404.83 ppm at the time of this writing [2]. The Intergovernmental Panel on Climate Change (IPCC [8]) reported in its fifth assessment report in 2014 (AR5 [9]) an average rate of increase in $CO_2$ of 1.4 ppm/year. Data by the Energy Information Agency (EIA, [10]) show worldwide $CO_2$ emissions from the consumption of coal were 13.8 billion metric tons in 2012, up from 8.0 billion metric tons two decades earlier, and there is no reason to expect this trend to stop any time soon.

The need to communicate climate science and the urgency of addressing the $CO_2$ problem have been recognized [11–15] but such efforts continue to meet with enormous obstacles [16].

$CO_2$ scrubbing involves the capture of $CO_2$ by a capture system (general capture reaction, GCR), the release of $CO_2$ from the substrate and its collection, and the long-term $CO_2$ sequestration [17]. $CO_2$ capture from air has been demonstrated [18], it is the pertinent tool to address $CO_2$ emissions from distributed sources [19–21], and $CO_2$ capture from the air is the method of last resort to combat excessive atmospheric $CO_2$ concentrations [22–24]. $CO_2$ scrubbing relies on chemical systems for reversible $CO_2$ capture [25,26] and usually involves carbamic acid formation (i.e., $CO_2$ reaction with amines [27–29], polyamine-based solid adsorbents [30,31], alkylamine-appended metalorganic framework [32–34], or diamine-appended metal-organic frameworks [35], and alternative systems [36]). Biomimetic $CO_2$ capture systems are of interest because they hold the promise to meet both the thermodynamic and the kinetic requirements for reversible $CO_2$ capture.

$$CO_2 + \text{Capture System} \rightleftarrows CO_2 - \text{adduct} \quad \text{(GCR)}$$

$$K_{eq}(\text{GCR}) = \frac{[CO_2 - adduct]}{[Capture\ System] \times [CO_2]}$$

$$CO_2 + \text{Carbonyl}\cdot H_2N - (\text{peptide}) - MgL_2 \cdot OH_2 \rightleftarrows CO_2 - \text{adduct} + H_2O \quad \text{(PCR)}$$

$$CO_2 + \text{Capture System} \rightleftarrows CO_2 - \text{adduct} + H_2O$$

$$K_{eq}(\text{RCR}) = \frac{[CO_2 - adduct] \times [H_2O]}{[Capture\ System] \times [CO_2]}$$

We have been interested in the development of rubisco-based biomimetic systems for reversible $CO_2$ capture from air. Our design of the chemical $CO_2$ capture and release systems is informed by the understanding of the binding of *the activator* $CO_2$ ($^{A}CO_2$) in rubisco (Figure 1) and the general strategy has been described [37,38]. Rubisco (ribulose 1,5-bisphosphate carboxylase/oxygenase, RuBisCO) catalyzes the addition of $CO_2$ and water to RuBP (d-ribulose 1,5-bisphosphate) in the photosynthetic carbon assimilation via the Calvin-Bassham-Benson cycle, and results in two molecules of 3-PGA (3-phospho-d-glycerate) and 0.5 $O_2$ [39,40]. Nearly all carbohydrate production in the biosphere depends on rubisco catalysis and rubisco is the most abundant protein on Earth. Form I rubisco contains eight large (L) and eight small (S) subunits, and the crystal structure of *Spinacia oleracea* [41,42] provided an early example of a hexa-decameric rubisco [43]. Form II rubisco lacks small subunits, generally occurs as $L_2$, and is exemplified by the bacterial rubisco of *Rhodospirillum rubrum* [44]. The mechanism of rubisco catalysis has been studied in detail [45,46] and these studies have established that rubisco must be activated by carbamylation of active-site lysine (Lys) with an activator $CO_2$ ($^{A}CO_2$). The carbamate formed is stabilized both by complexation to $Mg^{2+}$ and by NH$\cdots$OC hydrogen-bonding (Figure 1) and, importantly, the rubisco $^{A}CO_2$ capture (RCR) occurs with the release of a water molecule from the capture system.

In theoretical studies of reaction thermochemistry one usually computes the reaction enthalpy $\Delta H^\circ$ and the reaction entropy $\Delta S^\circ$ for the stoichiometric reaction at standard conditions (1 atm, 25 °C) and determines the reaction Gibbs free enthalpy via $\Delta G^\circ = \Delta H^\circ - T^\circ \cdot \Delta S^\circ$. This knowledge then allows for the computation of equilibrium concentrations, although this step is not usually applied in theoretical studies. For reactions with a severely limited reagent, one needs to consider the consequences of the non-stoichiometry on product formation. With an atmospheric $CO_2$ concentration of about 400 ppm, questions about the equilibrium concentration of $CO_2$ capture reactions have been asked frequently and they are entirely warranted. Hence, in this paper, we describe the determination of $CO_2$ capture equilibria as a function of $CO_2$ concentration. In addition, we describe temperature dependence of the $CO_2$ capture equilibria with a focus on the importance of the reaction entropy for effective $CO_2$ release at elevated temperature.

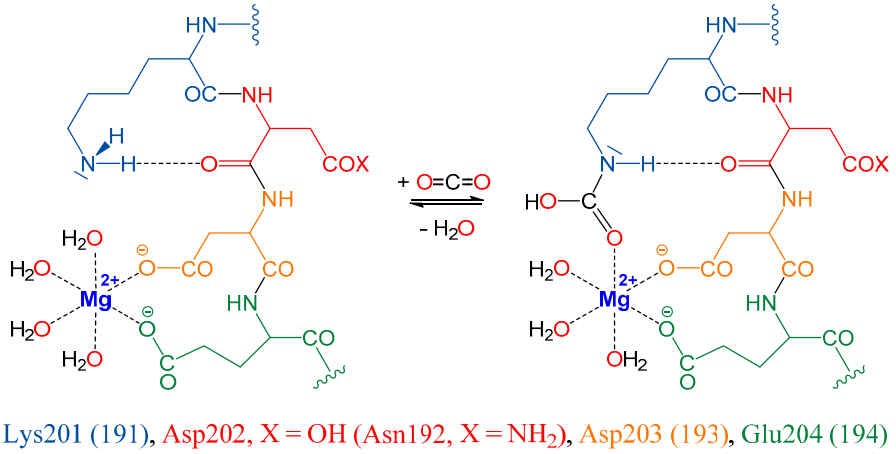


**Figure 1.** $CO_2$ capture in the active site of rubisco.

## 2. Results and Discussion

### *2.1. Capture Reaction Systems Studied*

We analyzed the thermochemistry of a rubisco-based small molecule model of the formation of *N*-methylcarbamic acid (NMCA) by addition of methylamine ($CH_3NH_2$) to $CO_2$, considering substrate and product stabilization by an active-side carbonyl model and complexation by a model metal complex $ML_2$ [37]. The model system is described by 14 reactions and the thermochemistry was determined at the B3LYP/6-31G* level for the natural case of magnesium $M^{2+} = Mg^{2+}$. Reaction R1 is the formation of NMCA ($H_3C{-}NH{-}CO{-}OH$) by addition of methylamine to $CO_2$ in the gas phase. Three effects of the environment need to be considered in the active site of rubisco (Figure 1) and these are (A) the stabilization of the product by hydrogen-bonding between NMCA and a model carbonyl compound; (B) the complexation of NMCA by a model metal complex $ML_2$; and (C) the forced replacement of ligand water by $CO_2$ at the metal center.

Importantly, the complexation of $CO_2$ to the metal cation $M^{2+}$ requires the replacement of a water molecule, and our analysis showed that this $H_2O/CO_2$ replacement is an essential feature of rubisco thermochemistry. The exchange of a ligand water molecule by a $CO_2$ molecule (reaction R10) is highly endergonic and this $H_2O/CO_2$ replacement penalty is required to lower the overall exergonicity of the $CO_2$ capture reaction and to allow overall reversibility. Reaction R14 models the capture of $CO_2$ and the addition of the $Mg^{2+}$-complexed $CO_2$ to a pre-positioned, carbonyl-aggregated methylamine $CH_3NH_2 \cdot (A/K)$ to form the $Mg^{2+}$-complexed and carbonyl-aggregated NMCA, $(A/K) \cdot NMCA \cdot ML_2$.

$$CO_2 + CH_3NH_2 \rightleftarrows NMCA \quad \text{(R1)}$$

$$H_2O \cdot MgL_2 + CO_2 + CH_3NH_2 \cdot FA \rightleftarrows \mathbf{17a} + H_2O \quad \text{(R14a)}$$

$$H_2O \cdot MgL_2 + CO_2 + CH_3NH_2 \cdot Ac \rightleftarrows \mathbf{21a} + H_2O \quad \text{(R14b)}$$

$$CO_2(g) \rightleftarrows CO_2(aq) \quad \text{(R15)}$$

We evaluated the RCR-reaction R14 with the model carbonyl formaldehyde (FA, R14a) and acetone (Ac, R14b), respectively. Molecular models of the $CO_2$-adducts **17a** (R14a) and **21a** (R14b) are shown in Figure 2, and the associated thermochemical parameters are listed in Table 1.

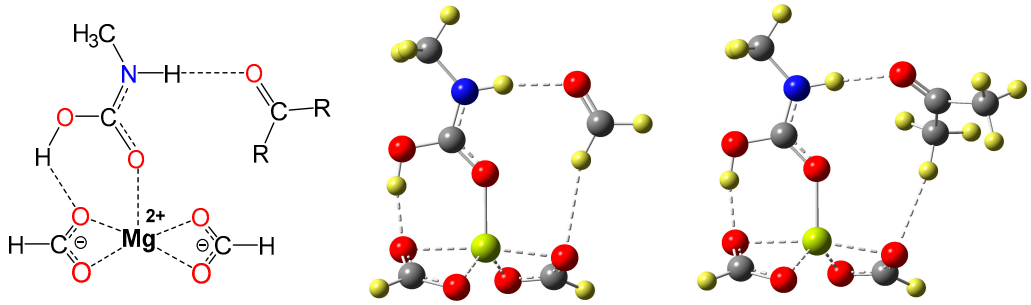


R = H: **17a**
R = $CH_3$: **21a**

**17a** **21a**

**Figure 2.** Molecular model of aggregates **17a** and **21a** formed between the magnesium formate $MgL_2$ complexed trans-trans isomer of *N*-methylcarbamic acid and model carbonyl formaldehyde (FA) or acetone (Ac), respectively. (Ball and Bond Type models are shown and color indicates elements: oxygen: red; nitrogen: blue; carbon: grey; hydrogen: yellow; magnesium: lime).

**Table 1.** Thermochemical data for capture systems. [1]

| Reaction | $\Delta G^\circ$ | $\Delta H^\circ$ | $\Delta S^\circ$ | Fraction $CO_2$-Adduct at $[CO_2]$ = 400 ppm | | |
|---|---|---|---|---|---|---|
| | | | | $T^\circ$ | $T^\circ$ + 20 | $T^\circ$ + 40 |
| R1 | 4.09 | −2.02 | −20.49 | | | |
| R14a | −6.59 | −17.26 | −35.79 | 0.0163 | 0.00159 | 0.000202 |
| R14b | −5.54 | −17.72 | −40.85 | 0.00281 | 0.000257 | 0.0000313 |
| R14h | −9.00 | −19.67 | −35.79 | 0.492 | 0.0676 | 0.00737 |
| HR1a | −6.59 | −15.00 | −28.21 | 0.0163 | 0.00204 | 0.000320 |
| HR1b | −6.59 | −20.00 | −44.98 | 0.0163 | 0.00120 | 0.000118 |
| HR1c | −6.59 | −25.00 | −61.75 | 0.0163 | 0.000705 | 0.0000435 |
| HR2a | −9.00 | −15.00 | −20.12 | 0.492 | 0.106 | 0.0184 |
| HR2b | −9.00 | −20.00 | −36.89 | 0.492 | 0.0654 | 0.00685 |
| HR2c | −9.00 | −25.00 | −53.66 | 0.492 | 0.0395 | 0.00254 |
| HR3a | −11.00 | −17.00 | −20.12 | 0.966 | 0.738 | 0.269 |
| HR3b | −11.00 | −22.00 | −36.89 | 0.966 | 0.623 | 0.119 |
| HR3c | −11.00 | −27.00 | −53.66 | 0.966 | 0.493 | 0.0499 |

[1] Gibbs free enthalpy $\Delta G^\circ$ and enthalpy $\Delta H^\circ$ in kcal/mol. Entropy $\Delta S^\circ$ in cal/(mol· K).

### 2.2. Equilibrium Concentrations with Non-Stoichiometric Conditions

The calculation of thermodynamic data for a given reaction with ab initio methods uses stoichiometric concentrations of the reagents. In the case of passive carbon capture, such an assumption does not accurately depict the relative concentrations of the reagents. Passive capture systems must operate at low pressures of $CO_2$, including the current atmospheric concentration (~400 ppm) [47].

$$K_H = \frac{[CO_2(aq)]}{P_{CO_2}} \quad (1)$$

Also, Henry's Law must be considered for aqueous carbon capture systems, because only dissolved $CO_2$ is available for binding. Henry's Law describes the proportion of gaseous $CO_2$ that enters the aqueous phase at equilibrium, illustrated in reaction (R15) and described by Equation (1). $K_H(T)$ is constant for a given gas and a given temperature; for $CO_2$ at room temperature this value has been experimentally determined to be $K_H(298.15) = K_H^0 = 0.034$ [48]. Using Henry's Law and the atmospheric pressure of $CO_2$, it is then simple to determine an approximate concentration of $CO_2$ in the aqueous phase of a passive capture system.

In this work, we primarily focus on the simple capture reactions (R1) and the rubisco capture reactions (R14). The product formation can be calculated using the equations for the equilibrium constants $K_{eq}$ for reactions (GCR) and (RCR), respectively. Defining the concentration of the capture system at equilibrium [CS] = $[CS]_0 - [CO_2\text{-CS}]$, where $[CO_2\text{-CS}]$ is the concentration of the $CO_2$-adduct formed and $[CS]_0$ is the initial concentration of the capture system, we obtain equations (2-GCR) and (2-RCR).

$$[CO_2 - CS] = \frac{[CS]_0 \times K_{eq} \times P_{CO_2} \times K_H}{1 + K_{eq} \times P_{CO_2} \times K_H} \quad \text{(2-GCR)}$$

$$[CO_2] = \frac{[CS]_0 \times K_{eq} \times P_{CO_2} \times K_H}{55.5 + K_{eq} \times P_{CO_2} \times K_H} \quad \text{(2-RCR)}$$

$$\frac{[CO_2 - CS]}{[CS]} = K_H \times P_{CO_2} \times e^{(-\Delta G/RT)} \quad \text{(3-GCR)}$$

$$\frac{[CO_2 - CS]}{[CS]} = \frac{K_H \times P_{CO_2} \times e^{(-\Delta G/RT)}}{55.5} \quad \text{(3-RCR)}$$

The isotherms in Figure 3 show the concentration of the $CO_2$-adduct formed $[CO_2\text{-CS}]$ as a function of the $CO_2$ pressure. This relationship produces isothermal curves with their asymptotic boundaries determined by the initial concentration of the capture system.

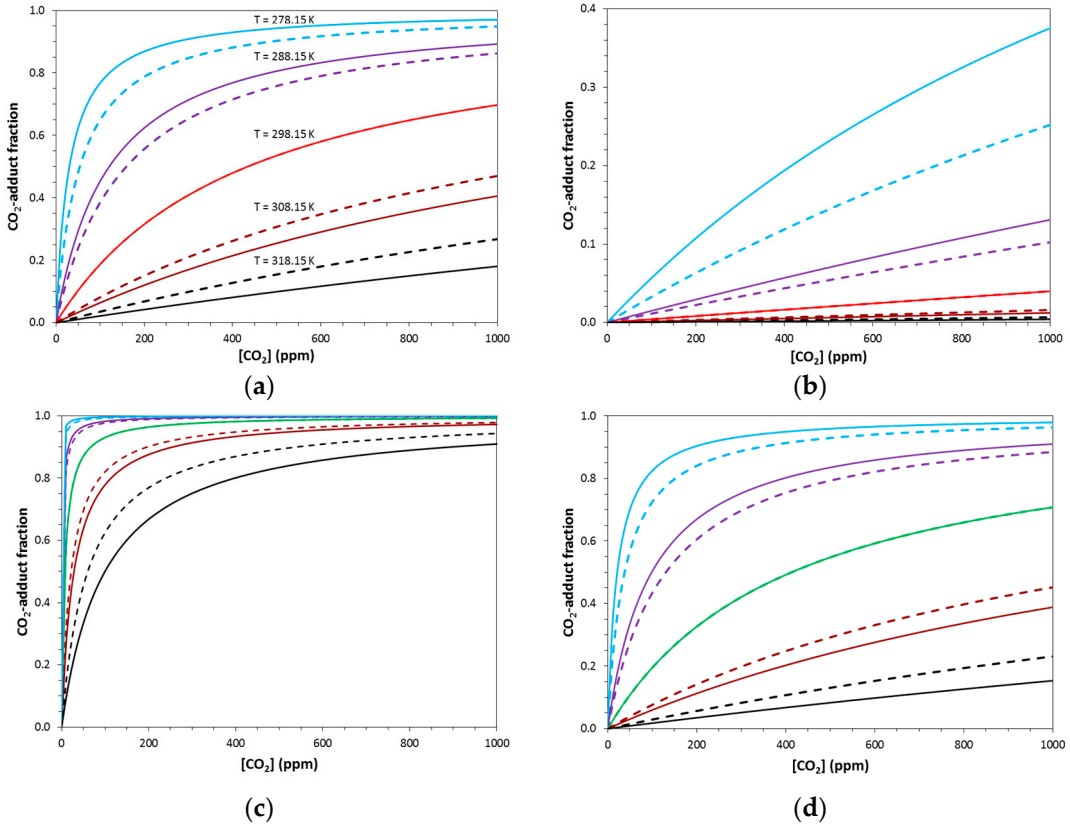


**Figure 3.** Equilibrium concentrations of complexed product of a general capture reaction (GCR) (**left**) and a rubisco-type capture reaction (RCR) (**right**) at five temperatures from 278.15 to 318.15 K. The color of the central curve (298.15 K) corresponds to the same system in Figures 3 and 4. Panels (**a**) and (**b**) describe the thermochemistry of R14a with $\Delta G^\circ = -6.59$ kcal/mol, $\Delta H^\circ = -17.26$ kcal/mol, and $\Delta S^\circ = -35.81$ cal/(mol·K). Panels (**c**) and (**d**) describe the thermochemistry of R14h with $\Delta G^\circ = -9.00$ kcal/mol, $\Delta H^\circ = -19.67$ kcal/mol, and $\Delta S^\circ = -35.79$ cal/(mol·K). Solid lines were computed with $T$-dependence of Henry's Law and dashed lines were computed without.

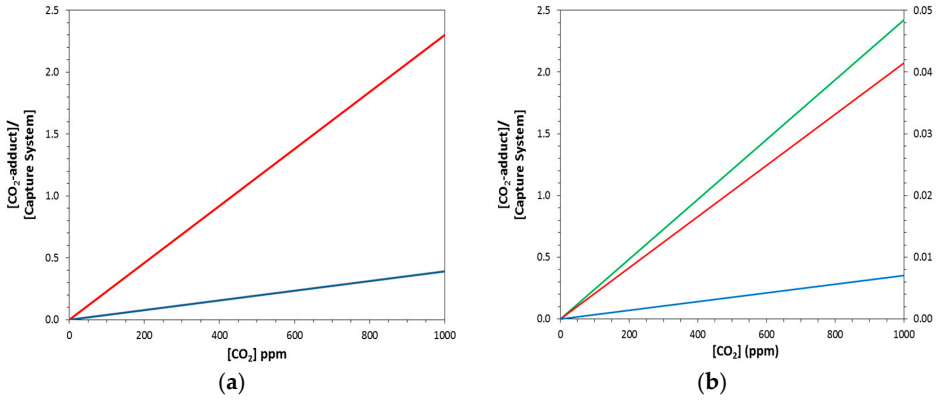


**Figure 4.** Carbon capture at 298.15 K for two carbon capture systems at near atmospheric concentrations. Gibbs free enthalpies of $\Delta G^\circ = -5.54$ kcal/mol (R14b, **blue**), $\Delta G^\circ = -6.59$ kcal/mol (R14a, **red**), and $\Delta G^\circ = -9.00$ kcal/mol (R14h, **green**). Plots for GCR are shown in (**a**) and plots for the RCR are shown in (**b**). To achieve a significant capture ratio in the RCR system requires a significantly more exergonic capture reaction; i.e., green in (**b**). The secondary axis in (**b**) allows for the recognition of the much diminished capture ratios for the less exergonic reactions (blue and red). The linear functions are as follows: (**a**) Blue; y = 3.91 × $10^{-4}$x, Red; y = 2.30· × $10^{-3}$x; (**b**) Blue; y = 7.05 × $10^{-6}$x, Red; y = 4.15 × $10^{-5}$x, Green; y = 2.42 × $10^{-3}$x.

The fraction of $CO_2$-adduct differs greatly in magnitude depending on the application of the GCR or RCR equations. The same thermochemical parameters afford much higher fractions computed with the GCR equation than with the correct RCR equation (Figure 3). The fractions computed with the RCR equations for reactions R14a (red) and R14b (blue) at [$CO_2$] = 400 ppm are listed in Table 1, and the respective values of 0.016 and 0.003 are very small. Obviously, our simplified theoretical model produces $\Delta G^\circ$ values that are not exergonic enough. Hence, we also studied the hypothetical reaction R14h with $\Delta G^\circ = -9$ kcal/mol. For this model system, we set $\Delta S^\circ$ (R14h) = $\Delta S^\circ$ (R14a) and obtain $\Delta H^\circ$ (R14h) = −19.67 kcal/mol. With R14h, we achieve a much more effective capture at room temperature (Figure 3d, green curve) and a very reasonable capture fraction of 0.492 (Table 1) at [$CO_2$] = 400 ppm.

Temperature affects the curvature of the fraction ($CO_2$-adduct) = f([$CO_2$]) isotherms in Figure 3 and we will discuss the $T$-dependence in more detail below (see Section 2.3). Instead of the fraction ($CO_2$-adduct), Figures 4 and 5 show the ratios [$CO_2$-CS]/[CS] as a function of [$CO_2$]. The ratios were computed with equations 3-GCR and 3-RCR, where $R$ is the gas constant (1.9858775 cal· $mol^{-1}\cdot K^{-1}$), $\Delta G$ is the Gibbs Free Enthalpy of the capture reaction at $T$, and $\Delta G = \Delta G^\circ$ for the special case of $T = T^\circ$. This ratio shows a linear dependence on the $CO_2$ pressure, and temperature affects the slope (but not the curvature).

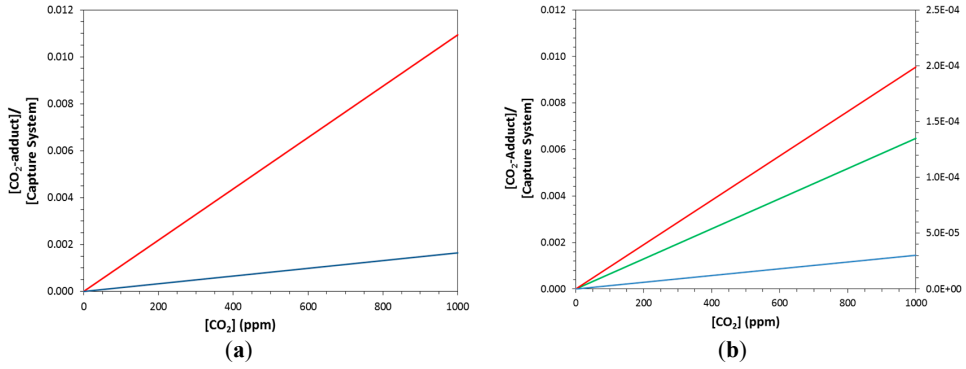


**Figure 5.** Carbon release at 348.15 K (= $T^\circ$ + 50) for two carbon capture systems at near atmospheric concentrations. Color indicates reaction thermochemical parameters; blue curves (R14b), red curves (R14a), and green curves (R14h). The linear functions are as follows: (**a**) GCR: y = 1.66 × $10^{-6}$x (**blue**); 1.10 × $10^{-5}$x (**red**). (**b**) RCR: y = 3.02 × $10^{-8}$x (**blue**); 1.99 × $10^{-7}$x (**red**); 6.48 × $10^{-6}$x (**green**).

The Gibbs free enthalpy of the capture reaction obviously will vary with temperature because of the entropy term, $\Delta G = \Delta H - T \cdot \Delta S$. The reaction enthalpy $\Delta H(T)$ and reaction entropy $\Delta S(T)$ depend on temperature only modestly and, for the temperature variations considered here, they can be approximated very well by $\Delta H(T) = \Delta H^{\circ}$ and $\Delta S(T) = \Delta S^{\circ}$. However, in our aqueous system temperature also significantly affects Henry's constant. This variation is described by the van't Hoff equation (Equation (4)), where the change in enthalpy of dissolution is a constant for a given gas. For $CO_2$ the value is $-\Delta_{sol}H/R$ = 2400 K. With this value, Equation (5) can be used to determine the value of the Henry's constant at temperature $T$ for $CO_2$.

$$\frac{d\ln K_H}{d\,(1/T)} = \frac{-\Delta_{sol}H}{R} \tag{4}$$

$$K_H\,(T) = K_H^o \times exp\left(\frac{-\Delta_{sol}H}{R}\left(\frac{1}{T} - \frac{1}{T^{\circ}}\right)\right) \tag{5}$$

For $-\Delta_{sol}H/R > 0$, it is clear that $CO_2$ will be better solvated at low temperatures and less solvated at temperatures higher than 298.15 K. This drives capture to be more effective at lower temperatures and release to be more effective at higher temperatures. The consequences of the $T$-dependence of Henry's constant are illustrated for specific cases in Figure 3, where solid lines were computed with $T$-dependence of Henry's Law and dashed lines without. In every panel, the dashed curves always are closer to the $T^{\circ}$-curve than the solid curves, that is, the load difference will always be increased by the $T$-dependence of Henry's constant.

### 2.3. Temperature Dependence of Capture Systems: Loading and Unloading

This illustration in Figure 6 is a rough schematic to consider the scale of the $CO_2$ capture in a *gedankenexperiment* (German: thought experiment). This apparatus is comprised of several square trays containing thin layers of aqueous capture solution. In order to capture large amounts of $CO_2$, the most important aspect is the volume of the capture system solution (CSS). To illustrate that a large volume is desired as well as a large surface area, a rack of shallow baths of solution was chosen to balance these two goals in a simple way. These thin layers are an attempt to acknowledge that the diffusion is a relevant and an important factor, but the schematic system is not optimized for diffusion because the main purpose of the *gedankenexperiment* is the thermodynamic analysis of slow processes. Because capture from ambient air occurs at very high dilutions of $CO_2$, it will not be a fast capture regardless. Of course, for fast capture at concentrated sources, the amount of $CO_2$ captured is controlled by kinetics and sophisticated chemical engineering solutions have been described that include more complicated gas/liquid contactor systems [49–52] and counter-current flow systems [53]. These systems vastly increase surface area-to-volume ratios and provide for surface renewal opportunities and facile gas diffusion. However, for passive capture from air the simplified apparatus of Figure 6 suffices to obtain a rough estimate of the amount of $CO_2$ that would be collected per load cycle.

$$Load = FW(CO_2) \times [CO_2 - CS]_{400} \times V_{CSS} \tag{6}$$

The load is determined by the volume of the capture system solution, the initial concentration of the amine capture system, and the temperature of the aqueous capture system. The *Load* can be calculated simply using Equation (6), where *Load* is the mass of captured $CO_2$ in g, $FW(CO_2)$ is the formula weight for $CO_2$, 44.01 g/mol, $[CO_2\text{-}CS]_{400}$ is the equilibrium concentration of product (mol/L) when the partial pressure of $CO_2$ is 400 ppm, and $V_{CSS}$ is the volume of the capture system solution (L). For an ideal capture system, the load should be highly dependent on the temperature so that $T$-variation may afford release under economic conditions. The fraction captured per cycle can be determined by comparison of the load data at capture and release temperatures (Table 1).

For a numerical illustration, we consider the trays of the apparatus to have a surface areas of 1 $m^2$ and to hold a solution with a depth of 2.5 cm. For a standard system of 10 layers of these trays, this

example results in a total solution volume of 250 L. Assuming an initial concentration of the capture system solution $[CS]_0$ = 0.1 M, the load is calculated using Equation (6). To find the concentration of the product, the initial concentration of the capture system solution is multiplied by the fraction of $CO_2$-adduct reported in Table 1. The amount of $CO_2$ collected in one capture cycle, the cycle load, equals the difference of the loads at the capture and release temperatures. With apparatus parameters being equal, the cycle load parallels the difference in the $CO_2$-adduct fractions at capture and release temperatures (cycle load fraction). In the case of capture system R14h, the free enthalpy is low enough to ensure binding at $T^\circ$ and the data in Table 1 show the fractions of $CO_2$-adduct to be 0.492 ($T^\circ$), 0.068 ($T^\circ$ + 20), and 0.007 ($T^\circ$ + 40). The fractions show that most $CO_2$ will be released when the temperature is raised by 20°, and that nearly all of the $CO_2$ will be released when the temperature is raised by 40°. The amount of $CO_2$ collected per cycle for a capture temperature of $T^\circ$ and release temperatures of $T^\circ$ + 20 and $T^\circ$ + 40 are 0.47 kg and 0.53 kg, respectively.

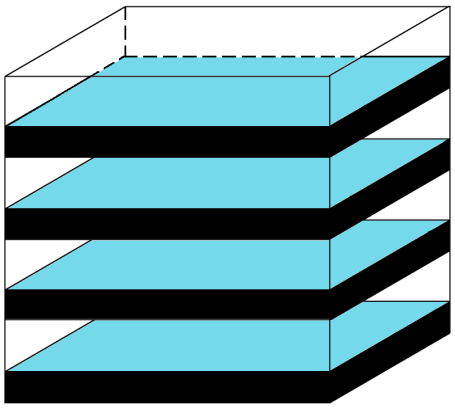

**Figure 6.** Schematic diagram of the carbon capture apparatus.

### *2.4. Variations of Thermodynamic Parameters—Guidelines for Capture System Design*

We modeled three sets of hypothetical reactions HR1−HR3 to explore the effectiveness of capture and release in dependence of the Gibbs free enthalpy and the capture reaction entropy (Table 1). The sets differ in the Gibbs free enthalpy with $\Delta G^\circ = -6.59$ kcal/mol for HR1 (as for R14a), $\Delta G^\circ = -9$ kcal/mol for HR2, and $\Delta G^\circ = -11$ kcal/mol for HR3. Within each set, we vary $\Delta H^\circ$ in steps of 5 kcal/mol. For HR1 and HR2, we use $\Delta H^\circ$ values of −15, −20, and −25 kcal/mol, respectively, and the $\Delta S^\circ$ values follow. The systems HR3 were constructed to share the $\Delta S^\circ$ values with HR2 and the $\Delta H^\circ$ values follow. With these parameters, we used equation 2-RCR to compute the fractions of $CO_2$-adduct at $[CO_2]$ = 400 ppm and $T^\circ$, $T^\circ$ + 20, and $T^\circ$ + 40, and the results are listed in Table 1.

Reaction HR1 is not sufficiently exergonic to produce adequate capture and Table 1 shows that all fractions are relatively low. Reactions HR2 and HR3, with their higher binding free enthalpies, demonstrate adequate capture, and these systems are illustrated in Figure 7.

Figure 7 shows the fractions of $CO_2$-adduct remaining bound at $T^\circ$ + 40 for the series of reactions HR2 and HR3, and this figure reveals the important role of entropy in the release process. As the reaction becomes more exentropic, the cycle yield improves in all cases, but the capture effectiveness is more complicated. For the most exentropic reaction of the HR2 series (HR2c), the fraction of $CO_2$-adduct remaining at $T^\circ$ + 40 is 0.003 and the unloading is highly effective. Even for the system HR2a, with its exentropicity mirroring that of the GCR R1, the unloading remains efficient: the fraction remaining is only 0.018 and the cycle load difference relative to HR2c is small (3.3%). Comparison of the HR2 series (Figure 7a) shows that at atmospheric pressure, the difference in capture due to entropy is functionally low.

In the more exergonic series of hypothetical reactions (HR3), the cycle load efficiency increases as with HR2 as the system becomes more exentropic. However, with the more exergonic reaction HR3,

the effect of entropy is drastically enhanced. Reaction HR3a is shown to have a fraction of $CO_2$-adduct of 0.269 at $T^\circ$ + 40 compared to HR3b with a fraction of 0.119 remaining. This corresponds to a 21.5% increase in cycle load for the more exentropic reaction. Further, the fraction of $CO_2$-adduct remaining for HR3c at the same temperature is 0.050. This is an 8.1% increase over HR3b and a 31.4% increase over HR3a. As illustrated by the increase in cycle load percentage across each series, the entropy effects for the more exergonic HR3 system are enhanced by a factor of nearly 10 over HR2.

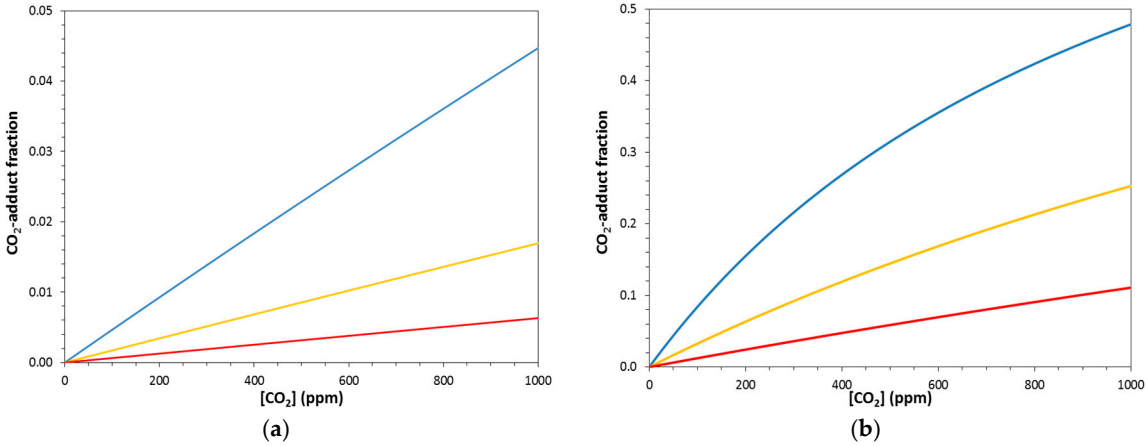


**Figure 7.** Fraction of $CO_2$-adduct remaining in capture solution at equilibrium at 338.15 K (= $T^\circ$ + 40) for the RCR-type reactions (**a**) HR2 with $\Delta G^\circ = -9$ kcal/mol and (**b**) HR3 with $\Delta G^\circ = -11$ kcal/mol. Reactions HR2 and HR3 are shown with entropies $\Delta S^\circ$ of −20.12 (**blue**), −36.89 (**yellow**), and −53.66 cal/(mol· K) (**red**).

After studying these hypothetical systems, it becomes pertinent to determine which would provide the best capture and the capture temperature plays an important role. We have already shown that $\Delta G^\circ = -6.59$ kcal/mol (R14a, HR1) is highly ineffective at $T^\circ$ and above, but as Figure 3b shows, at $T^\circ - 20$ (278.15 K) the system will have a $CO_2$-adduct fraction near 0.2. If we were to capture at $T^\circ - 20$ and release at $T^\circ$, the system will yield a relatively small but efficient cycle load. Even more useful at low temperatures would be a reaction with $\Delta G^\circ = -9$ kcal/mol (R14h, HR2). The most important feature of this hypothetical reaction is its variability around $T^\circ$. The fraction of $CO_2$-adduct captured of 0.492 at $T^\circ$ and [$CO_2$] = 400 ppm by this reaction is almost exactly between the two asymptotes. Because of this, it will vary greatly in capture with even small differences in temperature, as can be seen in Figure 3d. This great variability causes these reactions to be useful for low temperatures while they are less useful for higher temperatures. Considering R14h at $T^\circ - 20$ the fraction of $CO_2$-adduct is greater than 0.9 at [$CO_2$] = 400 ppm (Figure 3d). Raising the temperature to $T^\circ$ + 20 yields the fraction 0.068 (Table 1) and an excellent cycle load fraction of over 0.8. Even with a temperature variation from $T^\circ$ ($CO_2$-adduct fraction = 0.492) to $T^\circ$ + 20, a cycle load fraction of 0.4 is obtained, a good collection that requires minimal heating.

However when considering a capture at $T^\circ$ + 20 (45 °C), and release at $T^\circ$ + 40, the cycle load fraction will fall to 0.06, a very poor collection. Thus for higher temperature climates, a system with a more robust exergonicity is desired, for example $\Delta G^\circ = -11$ kcal/mol (HR3). HR3b at $T^\circ$ + 20 has a $CO_2$ capture fraction of 0.623, and increasing the temperature to $T^\circ$ + 40 (capture fraction of 0.119) yields a cycle load fraction of 0.504, a decent collection. Even better, for a capture at $T^\circ$ (capture fraction of 0.966) with release at $T^\circ$ + 40, the cycle load fraction is an excellent 0.847. At $T^\circ$ reaction HR3 already has a capture fraction of 0.966. Since the system cannot load significantly more $CO_2$ during capture, there is no benefit to using this system in a climate with a temperature cooler than 25 °C; in fact, the efficiency would suffer because more heat would be required to liberate the $CO_2$.

Our home state, Missouri, has great fluctuations in temperature through the seasons, so using a mixture of different capture systems may be most effective. In Columbia, Missouri, the average temperature in December is 0.78 °C which would indicate that a system with thermodynamic parameters similar to R14h would be best, while the average temperature in July is 25.4 °C, indicating that a reaction like HR3 would be considerably more effective [54]. For coastal or equatorial regions with less variation in temperature, the use of one capture system would be more feasible.

The considerations emphasize the significance of the magnitude of the entropy of the capture reaction. The large magnitude of reaction entropy of the capture reaction is a direct consequence of the presence of two capture moieties in the active site of rubisco and we offer an analogy with the illustration shown in Figure 8.

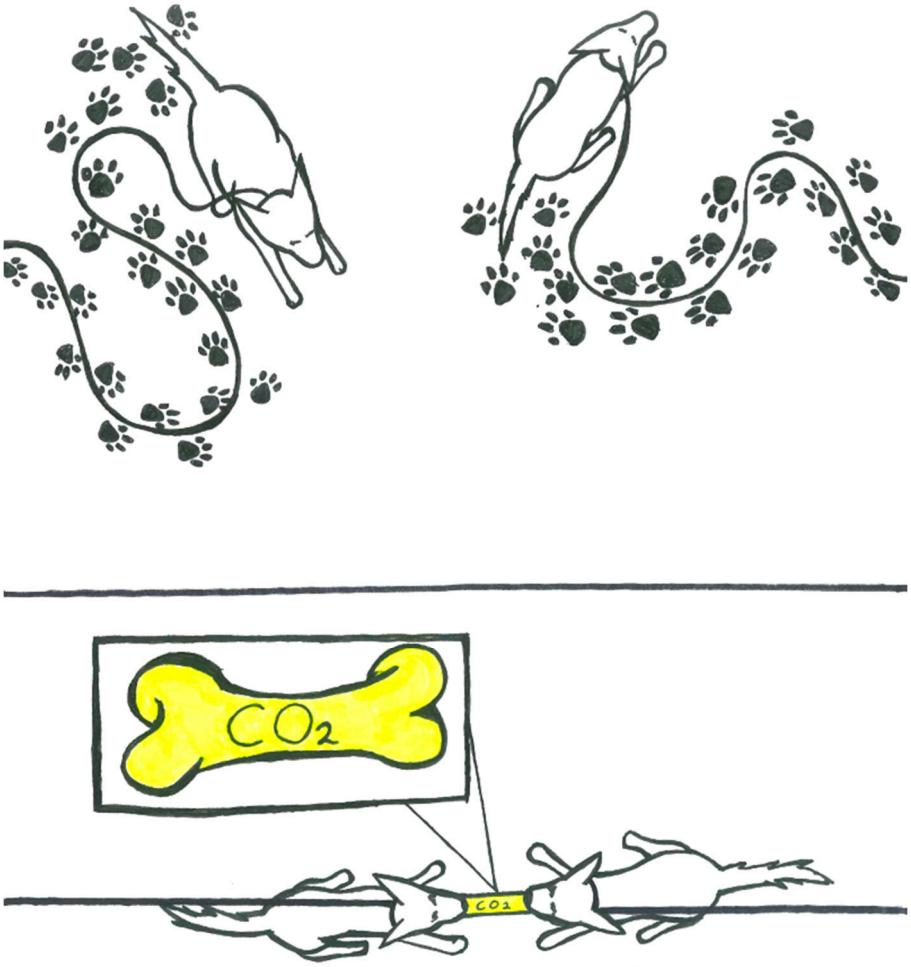


**Figure 8.** The genius of the rubisco-capture system stems from the large reduction of system entropy associated with bringing the two tethered capture moieties (the $Mg^{2+}$ site and the lysine amino group) together on $CO_2$ capture. The principle is well exemplified by the image of two leashed dogs biting on the same bone. In the absence of the bone, each dog enjoys great freedom in their accessible range (**illustration on top**). Biting on the same bone curtails the accessible range and the freedom of the dogs' mobilities (**bottom**).

## 3. Conclusions

In theoretical studies of chemical reactions with modern methods of electronic structure theory the reaction thermochemistry is usually reported for the stoichiometric reaction at standard conditions (1 atm, 25 °C) and the equilibrium constant $K_{eq}$ is related to the reaction Gibbs free enthalpy via $\Delta G^\circ = \Delta H^\circ - T^\circ \cdot \Delta S^\circ$. We described the computation of the equilibrium concentrations of the

$CO_2$-adducts for the general capture reaction GCR and the rubisco-type capture reaction (RCR) considering the atmospheric $CO_2$ concentration via Henry's law and as a function of temperature. The equations were applied to the thermochemistry of rubisco-based small molecule model reactions R1, R14a, and R14b, and three series of model reaction HR1–HR3 to illustrate the importance of the Gibbs free enthalpy for the effective capture and of the reaction entropy for economic $CO_2$ release at elevated temperature. Having a favorable capture of free enthalpy is of course an absolute necessity, but not all exergonic reactions are suitable $CO_2$ capture systems. Successful $CO_2$ capture systems must allow for effective release as well, and this feature is controlled by the reaction entropy. It is hoped that the presentation of the numerical examples provides useful guidelines for the design of more efficient capture systems.

The active site of rubisco employs two capture moieties to trap the activator $CO_2$. The metal site is attractive to any Lewis base, including water and $CO_2$, and their exchanges will be fast. Eventually, a $CO_2$ molecule will occupy a ligand site of $Mg^{2+}$ and it will then be trapped by Lewis-acid assisted nucleophilic addition of the amino-group of lysine to the heterocumulene $CO_2$. This two-pronged process allows for the capture of small amounts of $CO_2$ in a huge excess of water, and the mechanism has two major consequences for the thermochemistry. The endergonicity of the $H_2O/CO_2$ replacement is required to reduce the overall exergonicity of the $CO_2$ capture reaction and to allow overall reversibility. The second consequence for the RCR thermochemistry is the large reduction of system entropy which is associated with bringing the two tethered capture moieties (the $Mg^{2+}$ site and the lysine $NH_2$ group) together on $CO_2$ capture. This entropy feature is crucial for the success of the rubisco-based capture and release system. While chemists have a good sense of binding enthalpies, it is usually more challenging to appreciate reaction entropies, and with this in mind we offer an analogy in Figure 8. The principle of using a two-pronged capture system to ensure a large negative capture entropy can be exemplified by two leashed dogs biting on the same bone. In the absence of the bone, each dog has a large accessible range and they will enjoy the freedom to access much of their accessible space (high mobility, high entropy). Biting on the same bone curtails the accessible range and reduces the dogs' mobilities (low entropy). This principle also is highlighted by the graphical abstract.

**Acknowledgments:** Acknowledgment is made to the donors of the American Chemical Society Petroleum Research Fund for partial support of this research (#53415-ND4).

**Author Contributions:** Andrew Muelleman and Joseph Schell performed the research, computed the data, created Figures 1–7, and contributed to the writing. Spencer Glazer created the art work in the graphical abstract and Figure 8. Professor Rainer Glaser, Dipl.-Chem. guided the research and contributed to the writing.

**Conflicts of Interest:** The authors declare no conflict of interest.

## References

1. Keeling, R.F. Recording Earth's Vital Signs. *Science* **2008**, *319*, 1771–1772. [CrossRef] [PubMed]
2. Trends in Atmospheric Carbon Dioxide, US Department of Commerce, National Oceanic & Atmospheric Administration (NOAA), Earth System Research Laboratory, Global Monitoring Division. Available online: http://www.esrl.noaa.gov/gmd/ccgg/trends (accessed on 28 April 2016).
3. CarbonTracker CT2015, US Department of Commerce, National Oceanic & Atmospheric Administration (NOAA), Earth System Research Laboratory, Global Monitoring Division. Available online: http://www.esrl.noaa.gov/gmd/ccgg/carbontracker (accessed on 28 April 2016).
4. Peters, W.; Jacobson, A.R.; Sweeney, C.; Andrews, A.E.; Conway, T.J.; Masarie, K.; Miller, J.B.; Bruhwiler, L.M.P.; Pétron, G.; Hirsch, A.I.; et al. An atmospheric perspective on North American carbon dioxide exchange: CarbonTracker. *Proc. Natl. Acad. Sci. USA* **2007**, *104*, 18925–18930. [CrossRef] [PubMed]
5. CarbonTracker Documentation, CT2015 Release, CarbonTracker Team. 17 March 2016. Available online: http://www.esrl.noaa.gov/gmd/ccgg/carbontracker/CT2015_doc.pdf (accessed on 28 April 2016).
6. United States Carbon Cycle Science Program. Available online: http://www.carboncyclescience.gov (accessed on 28 April 2016).

7. OCO-2, Orbiting Carbon Observatory, NASA, Jet Propulsion Laboratory. Available online: http://oco.jpl.nasa.gov (accessed on 28 April 2016).
8. Intergovernmental Panel on Climate Change (IPCC). Available online: http://www.ipcc.ch (accessed on 28 April 2016).
9. IPCC, 2014: Climate Change 2014: Synthesis Report. In *Contribution of Working Groups I, II and III to the Fifth Assessment Report of the Intergovernmental Panel on Climate Change*; Core Writing Team, Pachauri, R.K., Meyer, L.A., Eds.; IPCC: Geneva, Switzerland, 2016; p. 151. Available online: http://www.ipcc.ch/report/ar5 (accessed on 28 April 2016).
10. Coal—Current Issues and Trends. EIA, U.S. Energy Information Agency. Available online: https://www.eia.gov (accessed on 28 April 2016).
11. Gore, A. *An Inconvenient Truth: The Planetary Emergency of Global Warming and What We Can Do about It*; Rodale Books: Emmaus, PA, USA, 2006.
12. Alliance for Climate Protection. Available online: https://www.change.org/organizations/climate_project (accessed on 28 April 2016).
13. 350.org. Available online: https://350.org (accessed on 28 April 2016).
14. The Carbon Bathtub. *National Geographic Magazine*. 2009. Available online: http://ngm.nationalgeographic.com/big-idea/05/carbon-bath (accessed on 28 April 2016).
15. Bringing $CO_2$ Monitoring to You: Communicating Atmospheric Chemistry. Available online: http://www.acs.org/content/acs/en/acs-webinars/professional-development/communicating-carbon.html (accessed on 28 April 2016).
16. Victor, D.G. *The Collapse of the Kyoto Protocol and the Struggle to Slow Global Warming*; Princeton University Press: New Jersey, NJ, USA, 2004.
17. IUPAC. *Compendium of Chemical Terminology*, 2nd ed.; Blackwell Scientific Publications: Oxford, UK, 1997; pp. 1342–1343.
18. First Successful Demonstration of Carbon Dioxide Air Capture Technology Achieved. By Earth Institute, Columbia University. Available online: physorg.com/news96732819.html (accessed on 28 April 2016).
19. Keith, D.W.; Ha-Duong, M.; Stolaroff, J.K. Climate strategy with $CO_2$ capture from the air. *Clim. Chang.* **2006**, *74*, 17–45. [CrossRef]
20. Lackner, K.S. Capture of carbon dioxide from ambient air. *Eur. Phys. J. Special Topics* **2009**, *176*, 93–106. [CrossRef]
21. Socolow, R.; Desmond, M.; Aines, R.; Blackstock, J.; Bolland, O.; Kaarsberg, T.; Lewis, N.; Mazzotti, M.; Pfeffer, A.; Sawyer, K.; et al. *Direct Air Capture of $CO_2$ with Chemicals: A Technology Assessment for the APS Panel on Public Affairs*; American Physical Society: Washington, DC, USA; 1; June; 2011; Available online: http://www.aps.org/policy/reports/assessments/upload/dac2011.pdf (accessed on 28 April 2016).
22. Zeman, F.S.; Lackner, K.S. Capturing carbon dioxide directly from the atmosphere. *World Resour. Rev.* **2004**, *16*, 62–68.
23. Lackner, K.S.; Brennan, S. Envisioning carbon capture and storage: Expanded possibilities due to air capture, leakage insurance, and C-14 monitoring. *Clim. Chang.* **2009**, *96*, 357–378. [CrossRef]
24. Lackner, K.S.; Brennan, S.; Matter, J.M.; Alissa Park, A.H.; Wright, A.; van der Zwaan, B. The urgency of the development of $CO_2$ capture from ambient air. *Proc. Natl. Acad. Sci. USA* **2012**, *109*, 13156–13162. [CrossRef] [PubMed]
25. Boot-Handford, M.E.; Abanades, J.C.; Anthony, E.J.; Blunt, M.J.; Brandani, S.; MacDowell, N.; Fernandez, J.R.; Ferrari, M.C.; Gross, R.; Hallett, J.P.; et al. Carbon capture and storage update. *Energy Environ. Sci.* **2014**, *7*, 130–189. [CrossRef]
26. Murphy, L.J.; Robertson, K.N.; Kemp, R.A.; Tuononen, H.M.; Clyburne, J.A.C. Structurally simple complexes of $CO_2$. *Chem. Commun.* **2015**, *51*, 3942–3956. [CrossRef] [PubMed]
27. Sun, Z.; Fan, M.; Argyle, M. Supported monoethanolamine for $CO_2$ separation. *Ind. Eng. Chem. Res.* **2011**, *50*, 11343–11349. [CrossRef]
28. Kuntz, J.; Aroonwilas, A. Performance of spray column for $CO_2$ capture application. *Ind. Eng. Chem. Res.* **2008**, *47*, 145–153. [CrossRef]

29. Idem, R.; Wilson, M.; Tontiwachwuthikul, P.; Chakma, A.; Veawab, A.; Aroonwilas, A.; Gelowitz, D. Pilot plant studies of the $CO_2$ capture performance of aqueous MEA and mixed MEA/MDEA solvents at the University of Regina $CO_2$ capture technology development plant and the Boundary Dam $CO_2$ capture demonstration plant. *Ind. Eng. Chem. Res.* **2006**, *45*, 2414–2420. [CrossRef]
30. Goeppert, A.; Czaun, M.; May, R.B.; Prakash, G.K.S.; Olah, G.A.; Narayanan, S.R. Carbon dioxide capture from the air using a polyamine based regenerable solid adsorbent. *J. Am. Chem. Soc.* **2011**, *133*, 20164–20167. [CrossRef] [PubMed]
31. Andreoli, E.; Barron, A.R. Effect of spray-drying and cryo-milling on the $CO_2$ absorption performance of $C_{60}$ cross-linked polyethyleneimine. *J. Mater. Chem. A* **2015**, *3*, 4323–4329. [CrossRef]
32. McDonald, T.; Lee, W.R.; Mason, J.A.; Wiers, B.M.; Hong, C.S.; Long, J.R. Capture of carbon dioxide from air and flue gas in the alkylamine-appended metal-organic framework mmen-$Mg_2$(dobpdc). *J. Am. Chem. Soc.* **2012**, *134*, 7056–7065. [CrossRef] [PubMed]
33. Sumida, K.; Rogow, D.L.; Mason, J.A.; McDonald, T.M.; Bloch, E.D.; Herm, Z.R.; Bae, T.-H.; Long, J.R. Carbon dioxide capture in metal-organic frameworks. *Chem. Rev.* **2012**, *112*, 724–781. [CrossRef] [PubMed]
34. Poloni, R.; Smit, B.; Neaton, J.B. Ligand-assisted enhancement of $CO_2$ capture in metal-organic frameworks. *J. Am. Chem. Soc.* **2012**, *134*, 6714–6719. [CrossRef] [PubMed]
35. McDonald, T.M.; Mason, J.A.; Kong, X.; Bloch, E.D.; Gygi, D.; Dani, A.; Crocella, V.; Giordanino, F.; Odoh, S.O.; Drisdell, W.S.; et al. Cooperative insertion of $CO_2$ in diamine-appended metal-organic frameworks. *Nature* **2015**, *519*, 303–319. [CrossRef] [PubMed]
36. Yang, Z.-Z.; Song, Q.-W.; He, L.-N. *Capture and Utilization of Carbon Dioxide with Poly-Ethylene Glycol, SpringerBriefs in Molecular Science*; Springer: New York, NY, USA, 2012.
37. Glaser, R.; Castello-Blindt, P.O.; Yin, J. Biomimetic Approaches to Reversible $CO_2$ Capture from Air. *N*-Methylcarbaminic Acid Formation in Rubsico-Inspired Models. In *New and Future Developments in Catalysis: Activation of Carbon Dioxide*, 1st ed.; Suib, S.L., Ed.; Elsevier: Amsterdam, The Netherlands, 2013; pp. 501–534.
38. Glaser, R. RuBisCO-Inspired Biomimetic Approaches to Reversible $CO_2$ Capture from Air. Metal Dependence of the $H_2O/CO_2$ Replacement Penalty. In *Advances in $CO_2$ Capture, Sequestration and Conversion*; Jin, F., He, L.-N., Hu, Y.H., Eds.; ACS Books: Washington, DC, USA, 2015; pp. 501–534.
39. Shively, J.M.; Van Keulen, G.; Meijer, W.G. Something about almost nothing: $CO_2$ fixation in chemautotrophs. *Ann. Rev. Microbiol.* **1998**, *52*, 191–230. [CrossRef] [PubMed]
40. Hugler, M.; Sievert, S.M. Beyond the Calvin cycle: Autotrophic carbon fixation in the ocean. *Ann. Rev. Marine Sci.* **2011**, *3*, 89–261. [CrossRef] [PubMed]
41. Taylor, T.C.; Andersson, I. Structure of a product complex of spinach ribulose-1,5-bisphosphate carboxylase/oxygenase. *Biochemistry* **1997**, *36*, 4041–4046. [CrossRef] [PubMed]
42. Taylor, T.C.; Andersson, I. Structural transitions during activation and ligand binding in hexadecameric Rubisco inferred from the crystal structure of the activated unliganded spinach enzyme. *Nat. Struct. Biol.* **1996**, *3*, 95–101. [CrossRef] [PubMed]
43. Gutteridge, S.; Newman, J.; Herrmann, C.; Rhoades, D. The crystal structures of Rubisco and opportunities for manipulating photosynthesis. *J. Exp. Botany* **1995**, *46*, 1261–1267. [CrossRef]
44. Lundqvist, T.; Schneider, G. Structure of the ternary complex of ribulose 1,5-bisphosphate carboxylase, magnesium(II) and activator carbon dioxide at 2.3 Å resolution. *Biochemistry* **1991**, *30*, 904–908. [CrossRef] [PubMed]
45. Hartman, F.C.; Harpel, M.R. Structure, function, regulation, and assembly of D-ribulose-1,5-bisphosphate carboxylase/oxygenase. *Annu. Rev. Biochem.* **1994**, *63*, 197–234. [CrossRef] [PubMed]
46. Cleland, W.W.; Andrews, T.J.; Gutteridge, S.; Hartman, F.C.; Lorimer, G.H. Mechanism of Rubisco: The carbamate as general base. *Chem. Rev.* **1998**, *98*, 549–561. [CrossRef] [PubMed]
47. Earth System Research Laboratory Global Monitoring Division. Available online: http://www.esrl.noaa.gov/gmd/ccgg/trends/ (accessed on 28 April 2016).
48. Sander, R. Compilation of Henry's law constants (version 4.0) for water as solvent. *Atmos. Chem. Phys.* **2015**, *15*, 4399–4981. [CrossRef]
49. Kumar, P.S.; Hogendoorn, J.A.; Feron, P.H.M.; Versteeg, G.F. New absorption liquids for the removal of $CO_2$ from dilute gas streams using membrane contactors. *Chem. Eng. Sci.* **2002**, *57*, 1639–1651. [CrossRef]

50. Dindore, V.Y.; Brilman, D.W.F.; Geuzebroek, F.H.; Versteeg, G.F. Membrane-solvent selection for $CO_2$ removal using membrane gas-liquid contactors. *Sep. Purif. Technol.* **2004**, *40*, 133–145. [CrossRef]
51. Atchariyawut, S.; Feng, C.; Wang, R.; Jiraratananon, R.; Liang, D.T. Effect of membrane Structure on mass-transfer in the membrane gas-liquid contacting process using microporous PVDF hollow fibers. *J. Membr. Sci.* **2006**, *285*, 272–281. [CrossRef]
52. Simons, K.; Nijmeijer, K.; Wessling, M. Gas-liquid membrane contactors for $CO_2$ removal. *J. Membr. Sci.* **2009**, *340*, 214–220. [CrossRef]
53. MacDowell, N.; Florin, N.; Buchard, A.; Hallett, J.; Galindo, A.; Jackson, G.; Adjiman, C.S.; Williams, C.K.; Shah, N.; Fennell, P. An overview of $CO_2$ capture technologies. *Energy Environ. Sci.* **2010**, *3*, 1645–1669. [CrossRef]
54. Climatological Data for St. Louis, Columbia, and Quincy—National Weather Service. Available online: http://www.weather.gov/lsx/cli_archive (accessed on 28 April 2016).